

# Chemical Bonds and Charge-Transfer Dynamics of a Dye–Hierarchical-TiO<sub>2</sub> Hybrid Interface

Carla Castellarin-Cudia,<sup>†,‡</sup> Tommaso Caruso,<sup>\*,§</sup> Enrico Maccallini,<sup>§</sup> Andrea Li Bassi,<sup>||,⊥</sup> Paolo Carrozzo,<sup>||</sup> Oreste De Luca,<sup>§</sup> Andrea Goldoni,<sup>†</sup> Victor Lyamayev,<sup>†,#</sup> Kevin Charles Prince,<sup>†,‡</sup> Federica Bondino,<sup>‡</sup> Elena Magnano,<sup>‡</sup> Raffaele Giuseppe Agostino,<sup>§</sup> and Carlo Spartaco Casari<sup>||,⊥</sup>

<sup>†</sup>Elettra-Sincrotrone Trieste S.C.p.A. s.s.14 km. 163.5, I-34149 Trieste, Italy

<sup>‡</sup>Istituto Officina dei Materiali, Consiglio Nazionale delle Ricerche, Laboratorio TASC, s.s.14 km. 163.5, I-34149 Trieste, Italy

<sup>§</sup>Consorzio Nazionale Interuniversitario per le Scienze Fisiche della Materia-Dipartimento di Fisica, Università della Calabria, Ponte Bucci, Cubo 33c, I-87036 Arcavacata di Rende, Italy

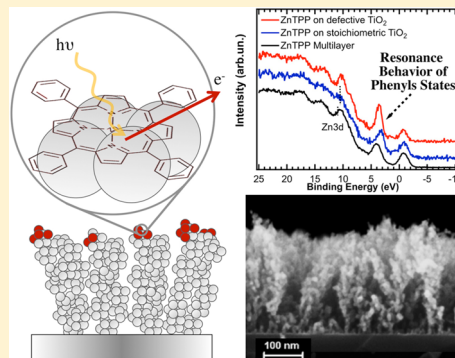
<sup>||</sup>Dipartimento di Energia and Center for Nano Engineered Materials and Surfaces, Politecnico di Milano, Via Ponzio, 34/3 I-20133 Milano, Italy

<sup>#</sup>Center for Nano Science and Technology at Polimi, Istituto Italiano di Tecnologia, Via Pascoli 70/3, 20133 Milano, Italy

<sup>#</sup>European XFEL GmbH, Notkestraße 85, 22607 Hamburg, Germany

## S Supporting Information

**ABSTRACT:** The adsorption of Zn-tetraphenylporphyrin (ZnTPP) on nanoporous hierarchically organized anatase TiO<sub>2</sub> structures and the properties of the corresponding hybrid interface were studied by synchrotron radiation experiments. The molecular structure, electronic properties, and bonding with nanostructured TiO<sub>2</sub> surfaces were analyzed by photoemission (XPS and UPS) and X-ray absorption spectroscopy (XAS). The charge transfer at the interface was investigated by means of valence band resonant photoemission experiments (ResPES) at the C K-edge. We show that the charge-transfer dynamics between the photoexcited ZnTPP and TiO<sub>2</sub> is strongly influenced by the presence of defects on the TiO<sub>2</sub> surface. On a stoichiometric anatase nanostructure, ZnTPP bonding occurs primarily via carbon atoms belonging to the molecular phenyl rings, and this creates a preferential channel for the charge transfer. This phenomenon is reduced in the case of defective TiO<sub>2</sub> surface, where ZnTPP interacts mainly through the molecule macrocycle. Our results represent a surface science study of the dye molecule behavior on a nanoporous TiO<sub>2</sub> photoanode relevant to dye-sensitized or hybrid solar cell applications, and they show the importance of the surface oxidation state for the charge-transfer process.



## 1. INTRODUCTION

Hybrid interfaces formed by organic molecules interacting with inorganic surfaces, such as metals or oxides, are attracting increasing interest for their fundamental role in novel devices, like solar cells, sensors, nanoelectronic and optoelectronic components. In dye-sensitized solar cells (DSSCs), light is absorbed by a dye molecule, and the electron–hole pair is separated at the interface with the inorganic surface. Then, the electron is injected into a TiO<sub>2</sub> photoanode.<sup>1,2</sup> DSSC device performance is strongly dependent on the efficiency of charge separation and on fast electron injection into the oxide. In turn, such phenomena are related to the complex interaction at the nanomolecular scale between the dye molecule and the oxide surface.

To this respect, the behavior of novel components is of great importance to assess the interest of new solutions for DSSC technology, comprising alternative dye molecules as well as innovative nano- and meso-photoanode architectures.

For example, by employing a customized zinc porphyrin molecule in conjunction with a cobalt (II/III) redox electrolyte instead of the usually employed ruthenium dyes and iodide/triiodide redox couple, a very high DSSC efficiency (12%) was obtained by M. Graetzel's group.<sup>3</sup> Moreover, photoanodes are typically made from micrometer-thick nanoparticle aggregates with high specific surface areas. 1D structures such as nanotubes, nanowires and nanorods of TiO<sub>2</sub> and ZnO were tested as possible alternatives,<sup>4–7</sup> with the aim of exploiting the preferential vertical transport path for the electrons and the possibility of light trapping/harvesting through proper management of light scattering. Recently, quasi-1D structures consisting of TiO<sub>2</sub> clusters hierarchically assembled in open/porous mesostructures resembling a forest of nanotrees were

Received: December 17, 2014

Revised: March 24, 2015

Published: March 25, 2015

fabricated and tested in DSSCs, showing improved electron lifetime and electrolyte diffusion<sup>8,9</sup> and, in solid state DSSC, showing improved performance because of light-trapping effects related to a hyperbranched morphology.<sup>10</sup>

More generally, porphyrins are attracting a lot of interest, among other molecular systems, for their overall properties. They are a vast family of molecules that play an important role in biological systems,<sup>11,12</sup> and their base structure consists of a macrocycle core, i.e., four pyrrole groups interconnected by mesobridge carbon atoms and several terminal groups attached externally to the core macrocycle. Accompanied by redox reactions, many metals can be inserted in the macrocycle center forming metallo-porphyrins. They efficiently absorb light in the visible range, showing electronic and adsorption properties on surfaces that can be tuned by modifying the metal ion center in the macrocycle and the terminal groups.<sup>13–15</sup> For example, in the case of ZnTPP (Zn-tetr phenylporphyrin) the molecule is terminated by four phenyl groups,<sup>16</sup> and a Zn atom occupies the molecular center, coordinated by four equivalent N atoms. In a thick ZnTPP film, the molecules interact by means of weak van der Waals forces, thus maintaining a structure similar to the one they have in the gas phase.<sup>17</sup>

A ZnTPP isolated molecule is then well-understood, and in literature, many works<sup>18–20</sup> were focused to its adsorption behavior on different substrates.

Here, we have studied the hybrid interface of a ZnTPP dye adsorbed *in situ* on a nanotree forest of TiO<sub>2</sub>, grown by pulsed laser deposition (PLD) with controlled morphology and structure down to the nanoscale. The study was accomplished by synchrotron radiation electron spectroscopies in order to gain insight into chemical bonding, electronic properties, and charge-transfer dynamics between ZnTPP monolayer and the TiO<sub>2</sub> substrate.

Adsorption of ZnTPP on single-crystal surfaces was already addressed by STM, XPS, NEXAFS, and ResPES experiments, investigating the substrate–molecule interaction, molecular orientation, surface and interface electronic properties, and charge-transfer dynamics.<sup>18–20</sup> In particular, these studies were carried out without the use of any additional linker between the organic molecule and the substrate. The molecule–substrate charge transfer is primarily driven by overlap of orbitals, therefore establishing a strong connection between adsorption geometry (i.e., coupling with the substrate) and charge injection. In detail, Castellarin-Cudia et al.<sup>19</sup> showed that ZnTPP adsorption orientation was different in the case of Si(111) and Ag(110) surfaces. In particular, ZnTPP macrocycle and phenyl rings lie flat on the Ag(110) surface, whereas they are rotated (the phenyls almost orthogonal) on Si(111). Consequently, the charge-transfer dynamics probed by ResPES were much stronger in the case of a ZnTPP monolayer adsorbed on Ag(110), whereas on Si(111) the ZnTPP monolayer ResPES spectra were more similar to those of the ZnTPP multilayer ones.

These experiments show the importance of understanding the dye adsorption geometry on the oxide surface. Some works have already addressed more realistic systems of Ru-based dyes on nanoporous TiO<sub>2</sub> even though there were many difficulties related to the ex situ sample preparation.<sup>21</sup> However, to the best of our knowledge, similar experiments have not been carried out for porphyrins on more realistic nanostructured oxide surfaces nor has the influence of surface oxidation state or chemical modification of the surface been addressed. In fact, even if single crystals represent good model systems because

they possess well-controlled and reproducible surfaces, molecular interactions with a nanoporous and cluster-assembled oxide can be radically different because of the complex nanoscale surface structure in contact with the molecules, e.g., different active facets, edges, defects at the crystallite boundaries and on the surface, absence of long-range order, and substoichiometric sites.

For the mentioned reasons, in this study, the ZnTPP adsorption and interface formation was addressed by investigating the properties of a monolayer of molecules on a hierarchically organized nanoscale TiO<sub>2</sub> substrate. To model different interfaces possibly occurring in a DSSC, the behavior of ZnTPP on surfaces with different oxygen stoichiometry, without changing the overall morphology, was studied. On the basis of our results, we propose a scheme for the molecule–substrate coupling and the factors that influence the charge-transfer dynamics between the photoexcited adsorbate and the oxide surface, which we found to be strongly related to the TiO<sub>2</sub> surface stoichiometry.

## 2. EXPERIMENTAL SECTION

Hierarchically assembled titanium oxide films with a thickness of about 200 nm were grown by PLD on Si substrates at room temperature by ablation of a Ti target (purity 99.99%) with UV nanosecond pulses from a KrF excimer laser ( $\lambda = 248$  nm, pulse duration 10–15 ns, 10 Hz repetition rate); the pulse energy was 300 mJ, corresponding to an energy density (fluence) of about 3 J/cm<sup>2</sup>. The deposition was carried out in an Ar/O<sub>2</sub> 4:1 mixture atmosphere under a total pressure of 30 Pa. The target–substrate distance was set at 58 mm, and the deposition rate was in the range 0.5–1 nm/s.

A postdeposition annealing treatment in air at 400 °C was carried out for 2 h in a muffle furnace to induce structural ordering (i.e., to transition from amorphous to anatase phase), as discussed in Di Fonzo et al.<sup>22</sup> The crystalline structure was checked by means of Raman spectroscopy with a Renishaw InVia spectrometer using the 514.5 nm wavelength of an argon ion laser.

At this stage, SEM images were acquired with a Zeiss Supra 40 field-emission scanning electron microscope. After preparation, samples were stored under static vacuum. For the synchrotron radiation spectroscopy experiments, the as-prepared stoichiometric TiO<sub>2</sub> surfaces were degassed in UHV at 300–350 °C for 30 min in order to remove any contaminants and then annealed at 320 °C for 60 min in oxygen ( $2 \times 10^{-6}$  mbar) in order to ensure a good oxidation. The surface stoichiometry was checked by XPS measurements. A defective surface, characterized by the presence of a number of Ti<sup>3+</sup> species associated with oxygen vacancies, was prepared by a further annealing in UHV at 600 °C for 15 min and checked by looking at the appearance of a feature at 1 eV in the valence band (VB) spectra.

In both cases, no changes in the anatase structure occur (Supporting Information).

High purity (99.95%) commercial ZnTPP (Sigma-Aldrich) was deposited on the TiO<sub>2</sub> samples *in situ* by a homemade evaporator made from Ta. To prepare the monolayer, a thick film was first sublimated in UHV and then annealed at 250 °C as described elsewhere.<sup>19,20</sup> This method was proven to form a ZnTPP monolayer on different monocrystalline substrates. Moreover, the thermal treatment at 250 °C in UHV does not change the stoichiometry of the substrate, as verified by XPS (Supporting Information).

Photoemission measurements were carried out at the Material Science (MS) and BACH beamlines at the Elettra synchrotron radiation facility in Trieste.<sup>23,24</sup> In both end stations, NEXAFS and XPS spectra were recorded in normal emission (NE) geometry with the incident beam at 60° relative to the surface normal. In XPS measurements, the overall spectral resolution was between 0.4 and 0.8 eV at ~500 eV photon energy. NEXAFS experiments at the C and N K-edges were acquired in Auger Yield mode. In ResPES experiments, VB spectra were acquired across the C K-edge at selected photon energies.

Great care was taken in monitoring beam-induced sample damage such as TiO<sub>2</sub> surface reduction, as already outlined in a previous study on similar samples.<sup>25</sup> Because both ZnTPP and TiO<sub>2</sub> were found to be sensitive to light exposure, we worked using a reduced flux, and we continuously checked the integrity of the system by XPS and VB measurements. In the following, we refer to the samples annealed in O<sub>2</sub> as stoichiometric TiO<sub>2</sub>, whereas defective TiO<sub>2</sub> indicates a sample annealed at 600 °C in vacuum.

The core-level photoemission spectra were referenced to the Ti 2p<sub>3/2</sub> core level of TiO<sub>2</sub> at 458.8 eV; the C 1s multilayer spectrum was fitted by four mixed Gaussian–Lorentzian (GL) lineshapes, fixing their relative intensity in the ratio 24:8:8:4 to mimic the theoretical carbon bonds present in ZnTPP (phenyl, pyrrolic C–C–N and C–C–C, and mesobridge C atoms) with the energies of the components reported in Castellarin Cudia et al.<sup>17</sup> as initial values for the fits. Furthermore, the FWHM was constrained to be equal for all the components. The GL width and the mixing ratio obtained in the multilayer fit were used as a basis for the monolayer curve-fitting analysis, whereas intensity and position were allowed to vary in a narrow range around the multilayer results. In addition, a few shake-up components were introduced to fit the multilayer spectrum well. N 1s spectrum was aligned and fitted in a similar way.

ResPES spectra were collected at the C K-edge of a ZnTPP multilayer as well as of ZnTPP monolayers deposited on a stoichiometric and a defective TiO<sub>2</sub> surface. All the data were normalized to the substrate Ti 3p peak intensity; moreover, in both monolayers the clean TiO<sub>2</sub> substrate signal was subtracted in order to focus on the ZnTPP electronic states' behavior. The energy alignment was done by using the Ti 3p (37.6 eV, BE scale) and Zn 3d lines (10.3 eV, BE scale).

### 3. RESULTS

**3.1. Properties of Hierarchically Structured TiO<sub>2</sub>.** PLD in a background atmosphere at the selected Ar/O<sub>2</sub> pressure of 30 Pa results in low-energy deposition and TiO<sub>2</sub> cluster nucleation, leading to a nanoporous assembly of nanoparticles about 10 nm in size that are characterized by a quasi-1D hierarchically organized assembly of nanoparticles resembling a forest of trees with <0.5 g/cm<sup>3</sup> density and a porosity of about 90%, as discussed by Di Fonzo et al.<sup>22</sup> An SEM image of the as-deposited film is shown in Figure 1a. In a previous work,<sup>25</sup> we showed that after thermal annealing in air the nanoparticles possess an anatase crystalline structure; for the investigated sample, the crystalline phase was checked by Raman spectroscopy (not shown). Annealing in air at 400 °C induces a slight densification, an increase in particle size, and an improved interparticle connection (see Figure 1b), without significantly affecting the mesoscale organization and morphology of the whole assembly.

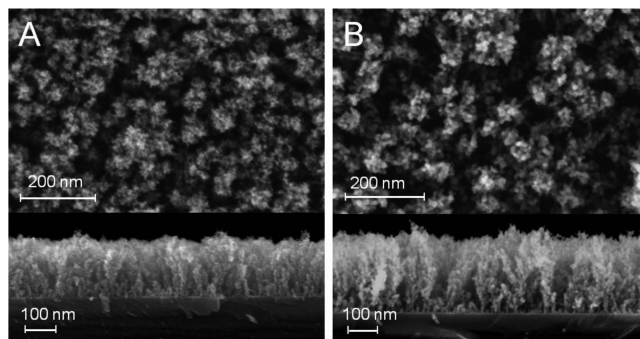


Figure 1. SEM pictures of (A) as-deposited and (B) annealed TiO<sub>2</sub> substrates.

The stoichiometry of the surface was checked by measuring the Ti 2p core levels (see Supporting Information) and the VB (Figure 2), showing almost no Ti<sup>3+</sup> contributions for the best oxidized surface. A well-defined defect state is instead seen for the substoichiometric defective samples; see the peak in Figure 2e at an energy of about 1 eV near the Fermi edge, attributed to oxygen vacancies.<sup>26</sup> It is evident in Figure 2 that in our samples

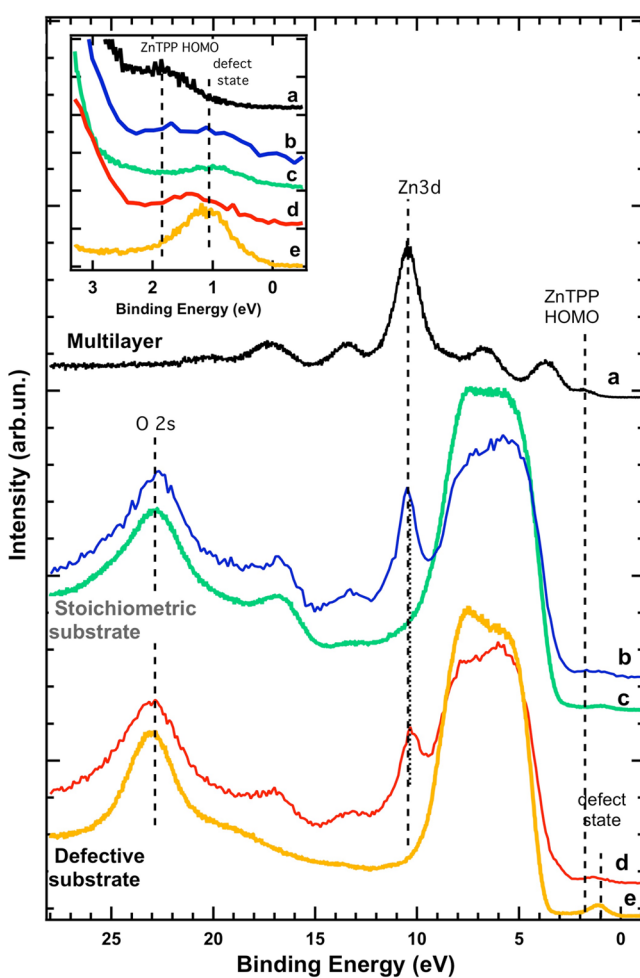


Figure 2. Valence band spectra (photon energy 170 eV) of (a, black) ZnTPP multilayer, (b, blue) ZnTPP monolayer on stoichiometric TiO<sub>2</sub>, (c, green) clean stoichiometric TiO<sub>2</sub>, (d, red) ZnTPP monolayer on defective TiO<sub>2</sub>, and (e, orange) clean defective TiO<sub>2</sub>. Inset, an enlargement of the region 0–4 eV is shown.

this feature is almost absent in stoichiometric  $\text{TiO}_2$  (Figure 2c) and quite intense in vacuum-annealed samples (Figure 2e).

### 3.2. Properties of ZnTPP/TiO<sub>2</sub> Hybrid Interfaces.

**3.2.1. Electronic Properties.** The VB spectra of a ZnTPP monolayer deposited on stoichiometric and defective  $\text{TiO}_2$  surfaces are shown in Figure 2 in comparison with the clean surfaces and the ZnTPP multilayer. The lowest energy region (0–5 eV) is enlarged and shown in the inset. The spectra are aligned to the Zn 3d level and normalized to the substrate related O 2s feature.

The ZnTPP HOMO in the multilayer case is located at 1.8 eV (Figure 2a), whereas the defect state in the defective clean  $\text{TiO}_2$  is at 1.1 eV (Figure 2e). These values are in line with those reported in literature.<sup>17,26</sup> The spectrum of the ZnTPP monolayer on defective  $\text{TiO}_2$  shows instead a peak located at ~1.4 eV (Figure 2d). This peak appears at a lower intensity and is slightly wider with respect to the defect state of the clean defective  $\text{TiO}_2$  (Figure 2e); this suggests that the peak at ~1.4 eV is the convolution of the ZnTPP HOMO at ~1.8 eV and the  $\text{TiO}_2$  3d defect state at 1.1 eV.

The ZnTPP monolayer on stoichiometric  $\text{TiO}_2$  (Figure 2b) shows a small and even wider peak in the range of 2–0 eV BE. Looking at the spectrum, we can assume that also in this case the feature is due to ZnTPP HOMO located slightly below 2.0 eV and a low-intensity  $\text{TiO}_2$  defect state at 1.1 eV. The presence of a defect state contribution in the VB may point to surface reduction following molecular adsorption (see below).

The ZnTPP HOMO is mainly located in the ZnTPP macrocycle so that if the molecule–substrate interaction is via the phenyl rings where part of the LUMO states are located then it would not be so evident in the VB spectrum that is strongly influenced by the substrate. Because of this, we also studied the LUMO levels by means of NEXAFS spectroscopy at the N K-edge, mainly to get information about the macrocycle because nitrogen is located there, and at the C K-edge, to get information about both the macrocycle and phenyl rings. From the literature,<sup>17,19,20</sup> it is known how to assign the contributions of the different features in the C K-edge NEXAFS spectrum to the different functional groups (macrocycle and phenyls) of the molecule, as also shown below. NEXAFS data are shown in Figure 3.

Figure 3a shows the N K-edge NEXAFS spectra of the analyzed cases: ZnTPP monolayers on stoichiometric and substoichiometric defective  $\text{TiO}_2$  and ZnTPP multilayer for comparison. No difference is observed between the LUMO levels of all the samples, suggesting a weak interaction between the porphyrin macrocycle and the substrates.

Figure 3b shows the NEXAFS spectrum collected at the C K-edge. In the literature,<sup>17,19,20</sup> the first band at 284.1 eV is assigned to transitions to the ZnTPP  $\pi^*$  LUMO level, which is known to be localized in the macrocycle; the second doublet peak at 285 eV is, instead, mainly due to  $\pi^*$  LUMO levels located on the phenyl rings. The remaining 287.3 and 288.3 eV peaks are due to  $\sigma$  bonds. Comparing the two monolayer spectra, we observe a difference in relative intensities of the bands. The intensity of transitions to the  $\sigma$  bond increases in the case of stoichiometric  $\text{TiO}_2$  surfaces with respect to the  $\pi^*$  feature localized on the phenyls, whereas the spectral line shape of the monolayer in the case of the defective surface is more similar to that of the multilayer one. These differences point to an electronic structure change driven by bonding with the substrate, i.e., a molecular electronic state rearrangement caused by direct orbital overlap ( $\sigma$  bond) among the phenyl groups

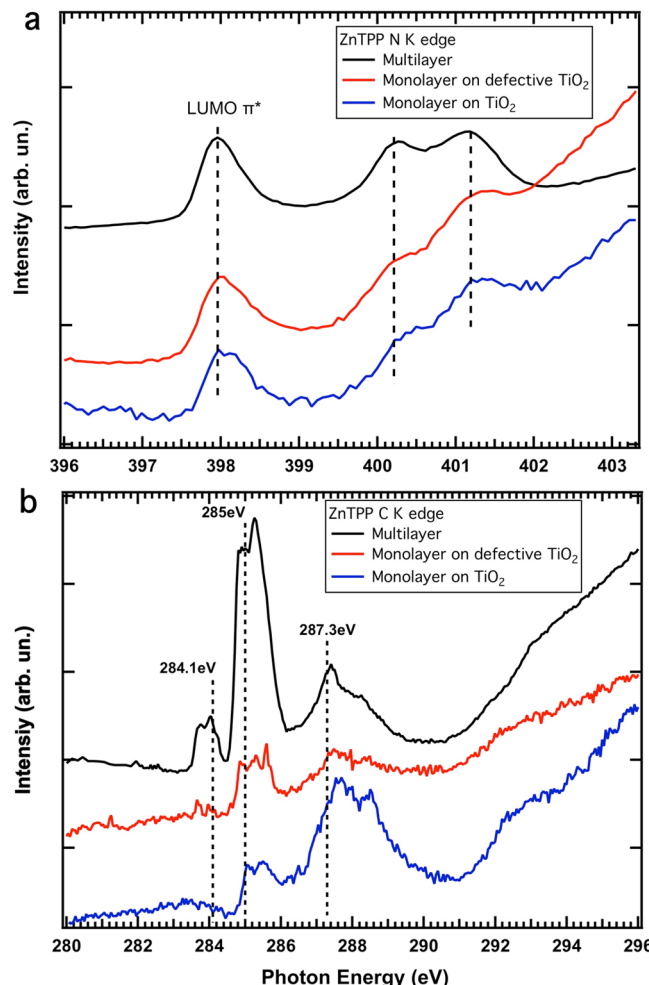


**Figure 3.** NEXAFS spectra: (a) N K-edge and (b) C K-edge. Dashed lines are a guide for the eye.

and stoichiometric  $\text{TiO}_2$ . (Orientation effects in this experiment can be neglected because of randomly oriented nanostructured surfaces.)

To better analyze the chemical bonding between  $\text{TiO}_2$  and ZnTPP, we carried out core-level spectroscopy by collecting C 1s and N 1s spectra for each case, as shown in Figure 4, where C 1s and N 1s photoelectron spectra and their fitted curves are reported.

The spectra in Figure 4a show the C 1s data. The multilayer spectrum served as a starting basis for analyzing the monolayer case (Experimental Section and Castellarin Cudia et al.<sup>17</sup>). At a first glimpse, the ZnTPP monolayer on stoichiometric  $\text{TiO}_2$  presents an extra feature at 285.8 eV that was absent in the ZnTPP multilayer. This feature is associated with C–O bonds<sup>27,28</sup> and thus can indicate a molecule–substrate bond, which involves the substrate oxygen and the carbon of the ZnTPP molecule. The intensity ratio between the other four components is also modified and deviates from the theoretical multilayer 24:8:8:4 ratio. The total C 1s band area was normalized to the 44 C atoms, and in Table 1, we report the average number of carbon atoms per bond found in the different samples. In the case of the ZnTPP monolayer on stoichiometric  $\text{TiO}_2$  surfaces, the molecule–substrate bonding feature (2.4 atoms) develops primarily at the expense of the phenyl ring component (21.5 atoms instead of 24). Then, on average, around 2.5 phenyl carbon atoms undergo bonding with

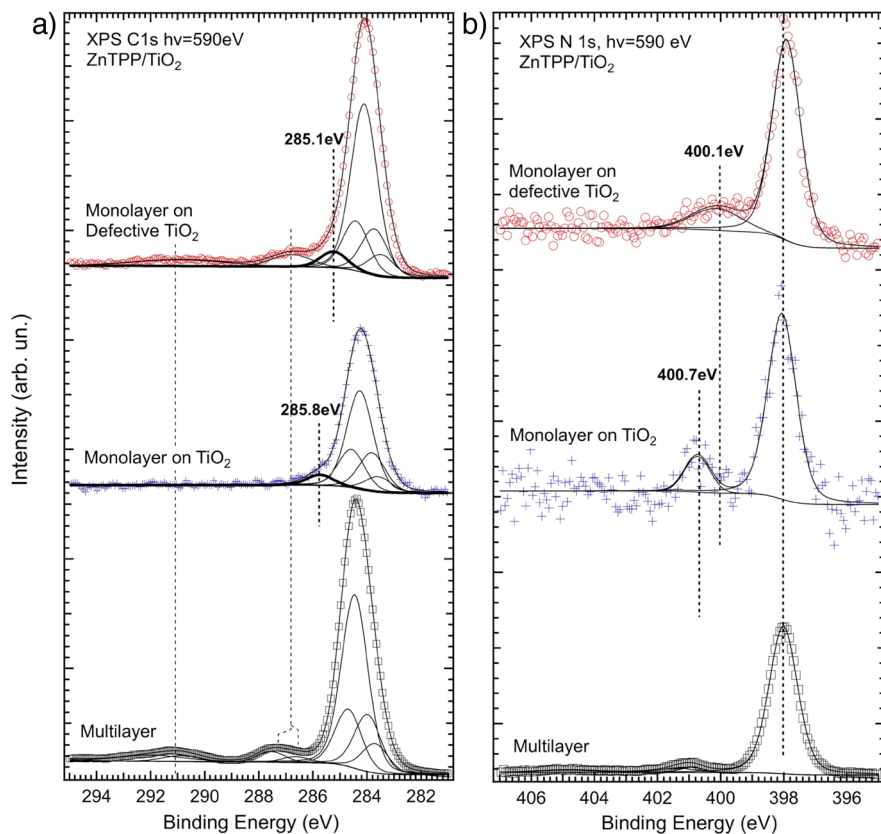


**Figure 4.** (a) C 1s and (b) N 1s core level photoelectron spectra from ZnTPP adsorbed on PLD TiO<sub>2</sub> films. Spectra are shown for a ZnTPP thick multilayer, ZnTPP monolayer on pristine TiO<sub>2</sub> surfaces, and a ZnTPP monolayer on a defective TiO<sub>2</sub> surface. The best fitting curves are shown for each spectrum.

**Table 1. Carbon Bonds within the ZnTPP/TiO<sub>2</sub> Systems<sup>a</sup>**

ZnTPP/TiO <sub>2</sub> components	multilayer	monolayer	monolayer on defective TiO <sub>2</sub>
Number of Atoms			
phenyl ring	24	21.5 ± 1.1	24.5 ± 0.6
pyrrolic C–C–N	8	8.4 ± 0.7	7.0 ± 0.2
pyrrolic C–C–C	8	8.4 ± 1.1	7.0 ± 0.2
C mesobridge	4	3.3 ± 0.7	2.8 ± 0.1
C–O bond		2.4 ± 0.7	2.6 ± 1.0

<sup>a</sup>Total number of carbon atoms was fixed at 44.

the oxidized substrate. The other three molecular components show smaller deviations with respect to the multilayer values. Errors in the best fit are still fairly high but are below the observed variations in the multilayer case.

The bonding is different for the defected substrate. The appearance of the bonding feature at 285.1 eV which can be considered also in this case as a C–O bond, is still observed with a similar intensity (2.6 atoms), but the affected molecular components (see Table 1) belong to electrons of the macrocycle (pyrrolic C–C–N and C–C–C, mesobridges C atoms), whereas the phenyl component weight seems unchanged by the ZnTPP adsorption and bonding on the defective surfaces. On average, pyrrolic C–C–N and C–C–C bonds and mesobridge carbon atoms all lower their spectral weight by around 1 atom following the bonding with TiO<sub>2</sub> defective surfaces.

As mentioned above, in addition to the main peaks, the ZnTPP C 1s spectra in Figure 4a show shake-up components

that are also affected by the substrate interaction. In particular, it is possible to observe a quenching of these components in the case of the monolayer on quasi-stoichiometric TiO<sub>2</sub>, compared to the multilayer case, whereas when adsorption is on the defective surface, the shake-up region is similar to the multilayer case, although less resolved. This supports the model of different ZnTPP/TiO<sub>2</sub> interaction mechanisms for the two surfaces.

Two components are needed to fit the N 1s region (Figure 4b), with the main peak at 398 eV resulting from the four ZnTPP-equivalent nitrogen atoms<sup>17</sup> and a second one at about 401 eV for the multilayer because of a π–π\* shake-up in the case of the ZnTPP multilayer. For the monolayer on the stoichiometric surface, the second peak is slightly shifted by 0.3 eV toward the main peak and also appears more intense. In the case of the monolayer on the defective surface, this peak is strongly shifted by 0.9 eV reaching 400.1 eV with respect to the shake-up, so it cannot be associated with the same transition. This component may originate from the contribution of bonds between N and undercoordinated Ti atoms.<sup>29</sup> Although the main peak falls essentially at the same binding energy for all the samples, indicating a similar overall chemical environment, the second peak suggests some changes, which are to be explained by also considering the C 1s spectrum results. A fraction of N atoms (slightly less than one-fifth) on the defective surface give clear evidence of the N-undercoordinated Ti bonds, suggesting interaction of the macrocycle core with the substrate surface. On the stoichiometric surface, the second peak can be explained by a superposition of shake-up components (as in the multilayer) and a second peak, due again to a (lower)

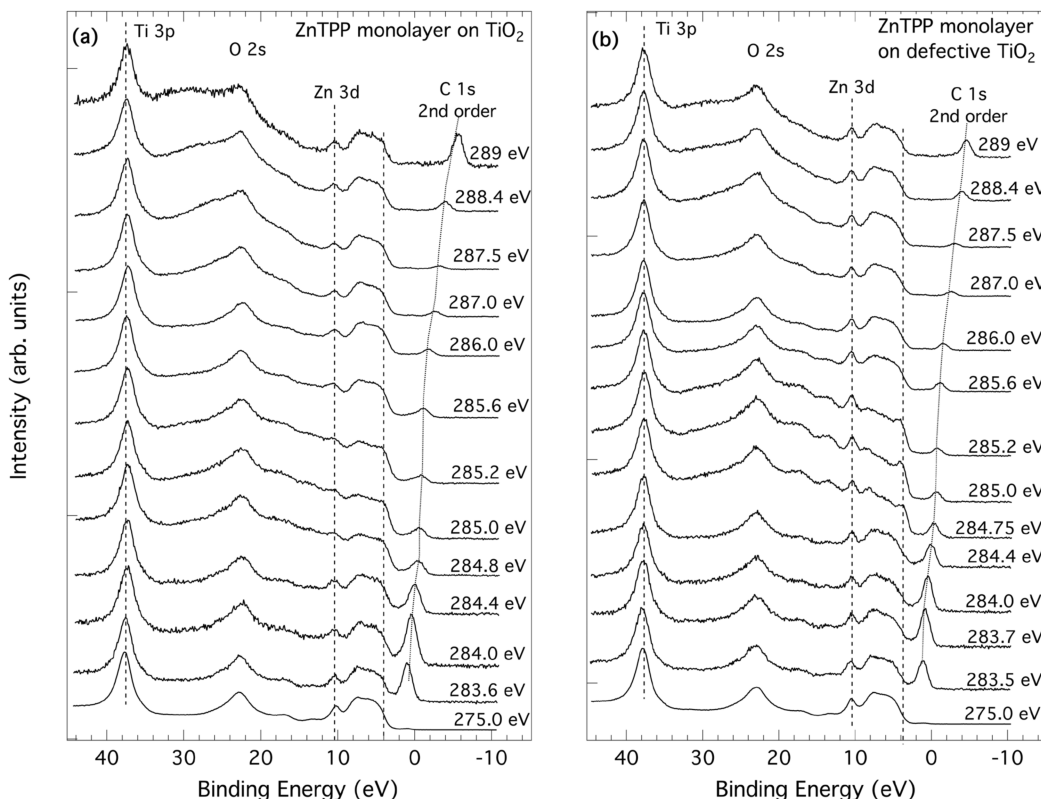


**Figure 5.** Resonant VB photoemission raw spectra: (a) ZnTPP monolayer on stoichiometric  $\text{TiO}_2$  and (b) ZnTPP monolayer on defective  $\text{TiO}_2$ . Note that the intensity of second-order radiation, exciting the C 1s electrons, is not constant relative to the first-order light exciting the VB states.

fraction of N atoms interacting with the substrate, although a more precise analysis cannot be done because of the superposition of the lines.

**3.2.2. Charge Transfer Dynamics.** We studied the charge-transfer dynamics by carrying out ResPES experiments.<sup>30–33</sup> This method can be viewed as analogous to a pump and probe technique: a core electron is excited to an empty state followed by a de-excitation process; the created core-hole is characterized by a lifetime that corresponds to a fixed time scale, allowing us to study the charge transfer with respect to this time scale. The de-excitation process gives rise to a resonant spectrum characterized by a normal, a spectator, and a Raman-participator Auger decay. The intensities of these resonances are measured, and information on dynamic charge transfer is obtained because the transferred charge does not contribute to the resonant spectrum, causing an intensity decrease of the resonant features.<sup>30–33</sup>

The experiment works in the following way: photon energies across a core-level edge are used to excite electrons, and for each excitation energy, a VB spectrum is collected. The integral of each electron spectrum as a function of photon energy is the NEXAFS spectrum, but each single VB spectrum allows the determination of the possible charge-transfer channels by analyzing the changes of the different features forming each spectrum. In the de-excitation process, the spatial overlap between the probed excited state and the conduction bands of the hosting substrate affects the balance between the various decay channels. In this way the charge-transfer dynamics can be monitored and the core hole lifetime, in the low-fs and sub-fs time regime, represents the time scale.<sup>30–33</sup>

From a single ResPES spectrum it is impossible to distinguish whether the excited electron delocalizes to the

substrate or to a neighbor atom belonging to the same molecule. As a consequence, in order to distinguish the molecule–molecule from the molecule–substrate delocalization, the ResPES spectra of monolayers are compared to one another and to those obtained on a thick film where only the weak electrostatic molecule–molecule interaction is involved.<sup>33</sup> Furthermore, because the photon energy is scanned across a core-level threshold, the chemical selectivity of the NEXAFS spectrum also applies to ResPES spectroscopy. In the case of the ResPES C K-edge spectrum of ZnTPP, it is possible to recognize which part of the molecule (phenyls/macrocyclic) is interacting with the substrate.

In Figure 5a,b, the resonant spectra are displayed at selected photon energies across the C K-edge for the two monolayers. Spectral features of both ZnTPP and  $\text{TiO}_2$  are present, and the Ti 3p and O 2s features are the most intense, whereas in the VB region (11–0 eV) the Zn 3d contribution at 10.3 eV overlaps other molecular components and the  $\text{TiO}_2$  substrate derived states. Compared with the VBS reported above (Figure 2), the substrate electronic states are the most intense in this photon energy region.

A spurious peak is also present in the spectra because of C 1s photoelectrons excited by second-order light. Unfortunately, it overlaps the features attributable to first-order-excited valence electrons near the Fermi level, usually the ZnTPP HOMO levels, and hampers the analysis of this energetic region.

From these data, we discern an interesting feature in the shoulder at around 4 eV in the main VB. This feature is almost absent in the off-resonance VBS (275 eV) and becomes more intense for photon energies of 284.8, 285.0, and 285.2 eV, whereas at higher photon energies, the shoulder has a lower intensity and its line shape does not change anymore. This

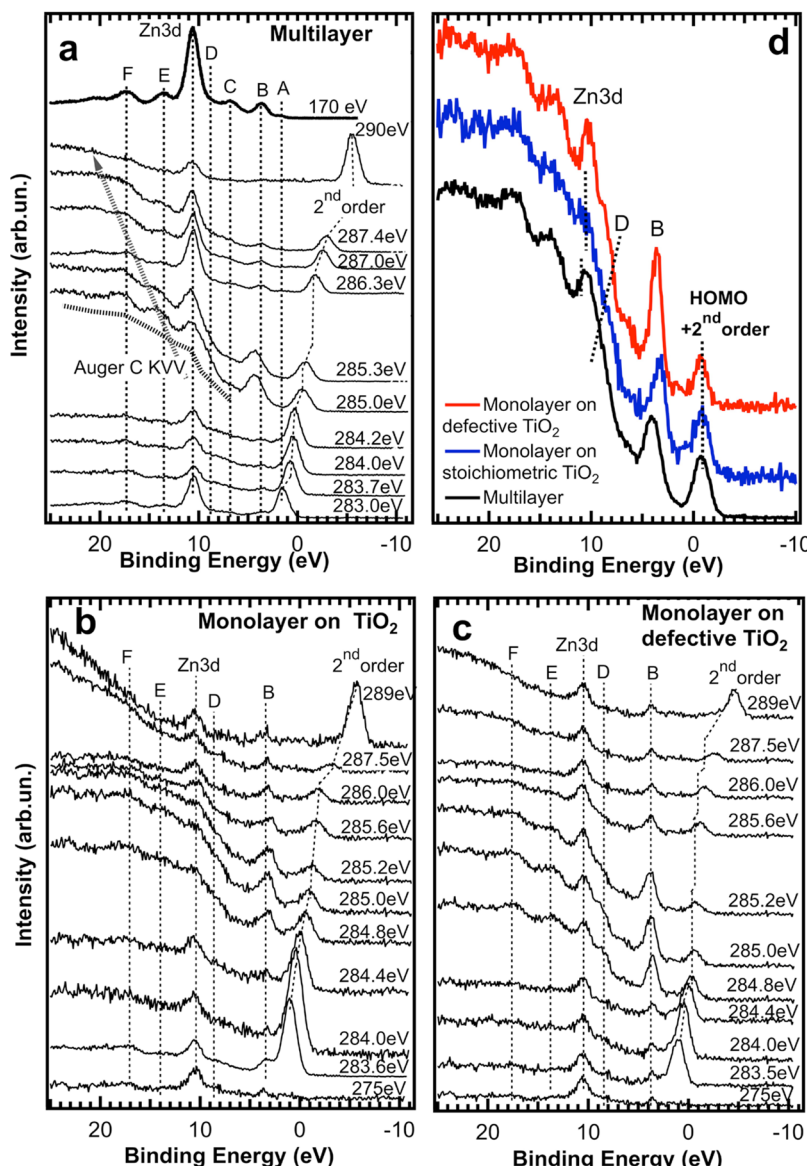


**Figure 6.** Resonant VB photoemission spectra; substrate signal was subtracted from the monolayer spectra reported in Figure 5: (a) multilayer, (b) ZnTPP monolayer on stoichiometric TiO<sub>2</sub>, and (c) ZnTPP monolayer on defective TiO<sub>2</sub>. (d) VB spectra measured at  $h\nu \sim 285.0$  eV for the cases a, b, and c.

behavior is observed for ZnTPP on both the stoichiometric (Figure 5a) and defective (Figure 5b) substrates.

To make a proper analysis of the resonant behavior of this feature, a TiO<sub>2</sub> substrate reference spectrum was subtracted from the raw spectra of Figure 5 to show only the ZnTPP molecular spectral features.

Data are reported in Figure 6 together with resonance VB spectra acquired on the multilayer ZnTPP thick film. Spectra show the Auger normal and spectator C KVV peak, i.e., the large feature that shifts in binding energy and increases in intensity with changing photon energy, the Zn 3d photoelectrons, and the features, labeled A, B, C, D, E, and F, due to molecular orbitals derived from N and C atom electronic states.

These features are particularly evident in the multilayer spectra but, although present, are somewhat difficult to discern in the monolayers because of a lower signal-to-noise ratio. The intensity change of these features with photon energy gives part of the resonant spectrum. In the case of charge transfer from

the molecules to the substrate, these features are quenched with respect to the multilayer case.

In Figure 6, interesting differences are observed by comparing the spectra of all three cases. In Figure 6a, the multilayer spectra are characterized by strong resonances corresponding to photon energy  $\sim 285.3$  eV, assigned to the excitation of C 1s electrons belonging to phenyl rings as shown by the NEXAFS spectrum (Figure 3). At that photon energy, several VB features are reproduced, but in particular, we note the state at 4–5 eV, labeled B in Figure 6a, which is particularly pronounced, together with D. This last one can be observed as a shoulder of the Zn 3d peak, even if it is not clearly distinguishable because of the increasing Auger signal.

The resonance spectra of the two monolayers are presented in Figure 6b,c. As for the multilayer case, the resonances appear when the C 1s of the phenyl rings are excited (284.8–285.2 eV); however, they have a different intensity. In particular, the B feature has the most recognizable behavior, and the spectra of Figure 6b,c give an overview of the resonant behavior. Figure

6d presents the spectra of all three cases at the same photon energy, ~285 eV.

It is evident that the B-state resonances in the case of monolayer on stoichiometric  $\text{TiO}_2$  are quenched with respect to those of the monolayer on defective  $\text{TiO}_2$ ; in the second case, the resonances more closely resemble those of the multilayer case. This different behavior points to a faster dynamic charge transfer (observed lower resonance intensity)<sup>30–34</sup> from the molecule toward the substrate in the case of the ZnTPP monolayer on stoichiometric  $\text{TiO}_2$ , rather than in the case of defective titania.

Concerning the other VB features, we observe a similar resonant behavior for the states named D, E, and F. The intensity enhancement happens when phenyl rings are excited, and this enhancement is higher when the ZnTPP molecules are bonded to a defective substrate. Similar considerations apply as in the case of state B, although the resonances of states D, E, and F are less strong.

#### 4. DISCUSSION

Formation of a Ti–O–C bond and the effect of chemical differences between  $\text{TiO}_2$  substrates have been reported in the literature. However, to our knowledge not many works report investigations of C–O bonding between benzene/phenyl carbon and  $\text{TiO}_2$  oxygen.

The TPP porphyrin phenyl rings are generally 60–75° rotated with respect to the molecular plane when adsorbed on a surface,<sup>19,20,32,33</sup> and the formation of a Ti–O–C bond, where C belongs to a phenyl ring that does not lie flat on a  $\text{TiO}_2$  anatase surface, has been described by Syres et al.,<sup>28</sup> who investigated dopamine deposited on  $\text{TiO}_2$  anatase. This molecule consists of a phenyl ring with two hydroxyl groups and one ethylamine chain, each of them bonded to one C of the phenyl ring. According to Syres et al., dopamine bonds to the  $\text{TiO}_2$  anatase surface through the oxygen atoms in a bidentate geometry, and the phenyl ring does not lie flat on the surface, being almost orthogonal to the substrate plane, thus forming a Ti–O–C bond. In this case, the oxygen belongs to the dopamine molecule instead of being a substrate oxygen; it replaces missing oxygens, forming bonds to an under-coordinated Ti, oxidizing it from  $\text{Ti}^{3+}$  to the  $\text{Ti}^{4+}$  state. The C–O bond that characterizes this molecule shows a geometry that is very similar to the present system: a C of the phenyl group is bonded to an oxygen surrounded by  $\text{Ti}^{4+}$  atoms. The authors report a BE of 285.9 eV for the C atoms that form the Ti–O–C bond, the value of which is quite close to ours.

In a similar manner, Syres et al.<sup>34</sup> have also analyzed pyrocatechol (1,2-dihydroxybenzene) on anatase  $\text{TiO}_2$  (101) and rutile (110), discovering the aromatic ring to be oriented at 27 and 23°, respectively, from the surface normal; this is another example of a benzene ring that does not lie flat on a  $\text{TiO}_2$  substrate and where the adsorption on the  $\text{TiO}_2$  (101) is in bidentate geometry.

Other molecules with no phenyl rings, which form C–O bonds with  $\text{TiO}_2$  surfaces, show different C1s BEs for the C in the C–O bond. As an example, the value points toward higher binding energies in the case of Ti–O–C bond formed by an alkene chain, as shown by Franking and Hamers.<sup>35</sup> Actually, they report data for alkenes adsorbed on rutile  $\text{TiO}_2$ , and they located the C1s BE of the carbon involved in the Ti–C–O bond at 286.2 eV.

From the fingerprint of C1s, we confirm the phenyl/substrate interaction and the absence of a macrocycle/substrate

interaction in the case of ZnTPP monolayer on stoichiometric  $\text{TiO}_2$ .

This is in line with the N 1s spectrum, which only in the case of defective  $\text{TiO}_2$  shows a shoulder at 400.2 eV and can be attributed to an N-undercoordinated Ti bond. Shao-Chun et al.<sup>29</sup> reported the synthesis of azobenzene via oxidation of anilines, and in this case, the effect is much more pronounced on defective  $\text{TiO}_2$  supports. After dissociation of anilines, they locate the N 1s energy of nitrogen in the N–Ti bond at ~400.5 eV, which is very close to the value found in our N 1s fitting results. This feature suggests the presence of a macrocycle/substrate interaction in our experiment on defective  $\text{TiO}_2$ . This interaction is not possible for stoichiometric  $\text{TiO}_2$  because there are no available electrons to bind to N, whereas they are present in the case of reduced  $\text{TiO}_2$ .

Finally, looking at the NEXAFS C K-edge spectrum of the ZnTPP monolayer on quasi-stoichiometric  $\text{TiO}_2$ , a lower intensity of the feature associated with phenyls with respect to the one associated with  $\sigma$  states is observed, suggesting a filling of the LUMO states located on the phenyl ring. Furthermore, in the same case the feature associated with the macrocycle at 284 eV is wider compared to the multilayer case. This could be due to the presence of a second feature at ~283 eV, which could be attributed to a new LUMO state resulting from the bonding between the phenyl ring and the substrate, as observed by Syres et al.<sup>28</sup> in the case of dopamine on anatase. They provide experimental and theoretical evidence of the existence of two new LUMO states at 281.7 and 282.8 eV, caused by the bonding of the molecule to the  $\text{TiO}_2$  substrate through a C–O–Ti bond. According to the authors, this bond gives rise to a different dynamic charge transfer without an  $e^-$ –hole separation in the dye, as normally happens in DSSCs.

They suggest a direct photoinjection of the electron from the dopamine to the conduction band of  $\text{TiO}_2$ . According to them, the charge transfer is due to the  $e^-$  excitation from the highest occupied  $\pi$  states of the dopamine to the  $\text{Ti}^{4+}$  (3d) levels, which are empty in the case of stoichiometric  $\text{TiO}_2$ . This would explain why the dynamic charge transfer is more favored in the case of stoichiometric  $\text{TiO}_2$  than in the case of a defective surface and why it concerns mainly the phenyl rings.

#### 5. CONCLUSIONS

In this paper, we reported a study of the interaction between nanostructured  $\text{TiO}_2$  anatase surfaces and ZnTPP dye molecules. We have shown how the interaction changes depending on  $\text{TiO}_2$  stoichiometry. As a consequence, different charge-transfer channels are opened, which lead to different charge-transfer mechanisms. In particular, the stoichiometric  $\text{TiO}_2$  surface favors the bonding of ZnTPP through the phenyl rings, opening a new dynamic charge-transfer channel, which allows the excited electron to move directly to the support conduction band. This effect is not equally efficient in the case of ZnTPP on the defective  $\text{TiO}_2$  surface. Our approach allowed us to deeply investigate the chemical bond between a model dye and a nanostructured  $\text{TiO}_2$  photoanode surface and to monitor the occurrence of charge transfer. A complete understanding of the complex interaction between organic dyes and oxides in a hybrid interface relevant for photovoltaic applications may help to identify suitable strategies to improve efficiency in a hybrid solar cell device.

## ■ ASSOCIATED CONTENT

### ● Supporting Information

X-ray absorption spectra ( $Ti\ L_{23}$  edge) and X-ray photoemission spectra ( $Ti\ 2p$  level) of nanoscale  $TiO_2$  substrates, as well as effects of thermal treatments. This material is available free of charge via the Internet at <http://pubs.acs.org>.

## ■ AUTHOR INFORMATION

### Corresponding Author

\*E-mail: Tommaso.caruso@fis.unical.it. Phone: 0039-(0)984-496095.

### Notes

The authors declare no competing financial interest.

## ■ REFERENCES

- (1) Cahen, D.; Hodes, G.; Gratzel, M.; Guillemoles, J. F.; Riess, I. Nature of Photovoltaic Action in Dye-Sensitized Solar Cells. *J. Phys. Chem. B* **2000**, *104*, 2053–2059.
- (2) Grätzel, M. Dye-Sensitized Solar Cells. *J. Photochem. Photobiol., C* **2003**, *4*, 145–153.
- (3) Yella, A.; Lee, H.; Tsao, H. N.; Yi, C.; Chandiran, A. K.; Nazeeruddin, M. K.; Diau, E. W.; Yeh, C.; Zakeeruddin, S. M.; Grätzel, M. Porphyrin-Sensitized Solar Cells with Cobalt (II/III)-Based Redox Electrolyte Exceed 12% Efficiency. *Science* **2011**, *334*, 629–634.
- (4) Cho, I. S.; Chen, Z.; Forman, A. J.; Kim, D. R.; Rao, P. M.; Jaramillo, T. F.; Zheng, X. Branched  $TiO_2$  Nanorods for Photoelectrochemical Hydrogen Production. *Nano Lett.* **2011**, *11*, 4978–4984.
- (5) Ko, S. H.; Lee, D.; Kang, H. W.; Nam, K. H.; Yeo, J. Y.; Hong, S. J.; Grigoropoulos, C. P.; Sung, H. J. Nanoforest of Hydrothermally Grown Hierarchical  $ZnO$  Nanowires for a High Efficiency Dye-Sensitized Solar Cell. *Nano Lett.* **2011**, *11*, 666–671.
- (6) Zhang, Q.; Dandeneau, C. S.; Zhou, X.; Cao, G.  $ZnO$  Nanostructures for Dye-Sensitized Solar Cells. *Adv. Mater.* **2009**, *21*, 4087–4108.
- (7) Zhang, Q.; Cao, G. Nanostructured Photoelectrodes for Dye-Sensitized Solar Cells. *Nano Today* **2011**, *6*, 91–109.
- (8) Sauvage, F.; Di Fonzo, F.; Li Bassi, A.; Casari, C. S.; Russo, V.; Divitini, G.; Ducati, C.; Bottani, C. E.; Comte, P.; Graetzel, M. Hierarchical  $TiO_2$  Photoanode for Dye-Sensitized Solar Cells. *Nano Lett.* **2010**, *10*, 2562–2567.
- (9) Divitini, G.; Stenzel, O.; Ghadirzadeh, A.; Guarnera, S.; Russo, V.; Casari, C. S.; Li Bassi, A.; Petrozza, A.; Di Fonzo, F.; Schmidt, V.; et al. Nanoscale Analysis of a Hierarchical Hybrid Solar Cell in 3D. *Adv. Funct. Mater.* **2014**, *24*, 3043–3050.
- (10) Passoni, L.; Ghods, F.; Docampo, P.; Abrusci, A.; Martí-Rujas, J.; Ghidelli, M.; Divitini, G.; Ducati, C.; Bindra, M.; Guarnera, S.; et al. Hyperbranched Quasi-1D Nanostructures for Solid-State Dye-Sensitized Solar Cells. *F. ACS Nano* **2013**, *7*, 10023–10031.
- (11) Hoard, J. L. Some Aspects of Metalloporphyrin Stereochemistry. *Ann. N.Y. Acad. Sci.* **1973**, *206*, 18–31.
- (12) Kadish, K. M.; Smith, K. M.; Gillard, R., Eds.; *The Porphyrin Handbook*; Academic: San Diego, CA, 2000.
- (13) Paulat, F.; Lehnert, N. Detailed Assignment of the Magnetic Circular Dichroism and UV-vis Spectra of Five-Coordinate High-Spin Ferric [Fe(TPP)(Cl)]. *Inorg. Chem.* **2008**, *47*, 4963–4976.
- (14) Vangberg, T.; Ghosh, A. A First-Principles Quantum Chemical Analysis of the Factors Controlling Ruffling Deformations of Porphyrins: Insights from the Molecular Structures and Potential Energy Surfaces of Silicon, Phosphorus, Germanium, and Arsenic Porphyrins and of a Peroxidase Compound I Model. *J. Am. Chem. Soc.* **1999**, *121*, 12154–12160.
- (15) Poveda, L. A.; Ferro, V. R.; De la Vega, J. M.; Gonzalez-Jonte, R. H. Molecular Modeling of Highly Peripheral Substituted Mg- and Zn-Porphyrins. *Phys. Chem. Chem. Phys.* **2000**, *2*, 4147–4156.
- (16) Adler, A. D.; Longo, F. R.; Finarelli, J. D.; Goldmacher, J.; Assour, J.; Korsakoff, L. A Simplified Synthesis for Mesotetraphenylporphine. *J. Org. Chem.* **1967**, *32*, 476.
- (17) Castellarin Cudia, C.; Vilmercati, P.; Larciprete, R.; Cepek, C.; Zampieri, G.; Sangaletti, L.; Pagliara, S.; Verdini, A.; Cossaro, A.; Floreano, L.; et al. Electronic Structure and Molecular Orientation of a Zn-Tetra-Phenyl Porphyrin Multilayer on Si(111). *Surf. Sci.* **2006**, *600*, 4013–4017.
- (18) Yoshimoto, S.; Tsutsumi, S.; Suto, K.; Honda, Y.; Itaya, K. Molecular Assemblies and Redox Reactions of Zinc(II) Tetraphenylporphyrin and Zinc(II) Phthalocyanine on Au(111) Single Crystal Surface at Electrochemical Interface. *Chem. Phys.* **2005**, *319*, 147–148.
- (19) Castellarin-Cudia, C.; Borghetti, P.; Di Santo, G.; Fanetti, M.; Larciprete, R.; Cepek, C.; Vilmercati, P.; Sangaletti, L.; Verdini, A.; Cossaro, A.; et al. Substrate Influence for the Zn-Tetraphenyl-Porphyrin Adsorption Geometry and the Interface-Induced Electron Transfer. *ChemPhysChem* **2010**, *11*, 2248–2255.
- (20) Vilmercati, P.; Castellarin-Cudia, C.; Gebauer, R.; Ghosh, P.; Lizzit, S.; Petaccia, L.; Cepek, C.; Larciprete, R.; Verdini, A.; Floreano, L.; et al. Mesoscopic Donor-Acceptor Multilayer by Ultrahigh-Vacuum Codeposition of Zn-Tetraphenyl-Porphyrin and  $C_{70}$ . *J. Am. Chem. Soc.* **2009**, *131*, 644–652.
- (21) Schwanitz, K.; Weiler, U.; Hunger, R.; Mayer, T.; Jaegermann, W. Synchrotron-Induced Photoelectron Spectroscopy of the Dye-Sensitized Nanocrystalline  $TiO_2$ /Electrolyte Interface: Band Gap States and Their Interaction with Dye and Solvent Molecules. *J. Phys. Chem. C* **2007**, *111*, 849–854.
- (22) Di Fonzo, F.; Casari, C. S.; Russo, V.; Brunella, M. F.; Li Bassi, A.; Bottani, C. E. Hierarchically Organized Nanostructured  $TiO_2$  for Photocatalysis Applications. *Nanotechnology* **2009**, *20*, 015604.
- (23) Vasina, R.; Kolarik, V.; Dolezel, P.; Mynar, M.; Vondracek, M.; Chab, V.; Slezak, J.; Comicioli, C.; Prince, K. C. Mechanical Design Aspects of a Soft X-ray Plane Grating Monochromator. *Nucl. Instrum. Methods Phys. Res., Sect. A* **2001**, *467*–468, 561–564.
- (24) Zangrandi, M.; Zucchinelli, M.; Finazzi, M.; Cocco, D.; Rochow, R.; Parmigiani, F. Polarized High-Brilliance and High-Resolution Soft X-ray Source at ELETTRA: The Performance of Beamline BACH. *Rev. Sci. Instrum.* **2004**, *75*, 1.
- (25) Fusi, M.; Maccallini, E.; Caruso, T.; Casari, C. S.; Li Bassi, A.; Bottani, C. E.; Rudolf, P.; Prince, K. C.; Agostino, R. G. Surface Electronic and Structural Properties of Nanostructured Titanium Oxide Grown by Pulsed Laser Deposition. *Surf. Sci.* **2011**, *605*, 333–340.
- (26) Diebold, U. The Surface Science of Titanium Dioxide. *Surf. Sci. Rep.* **2003**, *48*, 53–229.
- (27) McCafferty, E.; Wightman, J. P. Determination of the Concentration of Surface Hydroxyl Groups on Metal Oxide Films by a Quantitative XPS Method. *Surf. Interface Anal.* **1998**, *26*, 549–564.
- (28) Syres, K. L.; Thomas, A.; Bondino, F.; Malvestuto, M.; Graetzel, M. Dopamine Adsorption on Anatase  $TiO_2$ (101): A Photoemission and NEXAFS Spectroscopy Study. *Langmuir* **2010**, *26*, 14548–14555.
- (29) Li, S. C.; Diebold, U. Reactivity of  $TiO_2$  Rutile and Anatase Surfaces toward Nitroaromatics. *J. Am. Chem. Soc.* **2010**, *132*, 64–66.
- (30) Brühwiler, P. A.; Karis, O.; Martensson, N. Charge-Transfer Dynamics Studied Using Resonant Core Spectroscopies. *Rev. Mod. Physics* **2002**, *74*, 703.
- (31) Schnadt, J.; Brühwiler, P. A.; Patthey, L.; O'Shea, J. N.; Soedergren, S.; Odelius, M.; Ahuja, R.; Karis, O.; Baessler, M.; Persson, P.; et al. Experimental Evidence for Sub-3-fs Charge Transfer from an Aromatic Adsorbate to a Semiconductor. *Nature* **2002**, *418*, 620.
- (32) Vilmercati, P.; Cvetko, D.; Cossaro, A.; Morgante, A. Heterostructured Organic Interfaces Probed by Resonant Photoemission. *Surf. Sci.* **2009**, *603*, 1542–1556.
- (33) Vilmercati, P.; Castellarin-Cudia, C.; Larciprete, R.; Cepek, C.; Zampieri, G.; Sangaletti, L.; Pagliara, S.; Verdini, A.; Battocchio, C.; Polzonetti, G.; et al. Molecular Orientations, Electronic Properties and Charge Transfer Timescale in a Zn-Porphyrin/ $C_{70}$  Donor-Acceptor Complex for Solar Cells. *Surf. Sci.* **2006**, *600*, 4018–4023.

- (34) Syres, K. L.; Thomas, A. G.; Flavell, W. R.; Spencer, B. F.; Bondino, F.; Malvestuto, M.; Preobrajenski, A.; Graetzel, M. Adsorbate-Induced Modification of Surface Electronic Structure: Pyrocatechol Adsorption on the Anatase  $\text{TiO}_2$  (101) and Rutile  $\text{TiO}_2$  (110) Surfaces. *J. Phys. Chem. C* **2012**, *116*, 23515–23525.
- (35) Franking, R.; Hamers, R. J. Ultraviolet-Induced Grafting of Alkenes to  $\text{TiO}_2$  Surfaces: Controlling Multilayer Formation. *J. Phys. Chem. C* **2011**, *115*, 17102–17110.